Journal of Advances in Science and Technology
Vol. 19, Issue No. 2, April-2022, ISSN 2230-9659

DOI: https://doi.org/10.29070/zfya1g64

Check for updates

Welding of Different Metals Across Ferritic Substrates: A Thermal Modeling

Sagar Arun Rao Deshmukh [1] , Dr. Prashan Jagannath Patil [2]

1. Research Scholar, Sunrise University, Alwar, Rajasthan, India ,
2. Associate Professor(Dept. of Engineering), Sunrise University, Alwar, Rajasthan, India

Abstract: In the modern era, scientists are able to accurately predict the microstructural evolution ofcomplex metallurgical systems, including the formation of phases at elevated temperatures over l.ongperiods of time. Those calculations are useful because they provide insight without the need forlaborious and costly experiments. Computational simulations are especially useful in the powergeneration industry, where the service parameters have a significant impact on the materials used.Dissimilar metal welds (DMWs) ranging in hardness from T23 to T91 will be the focus of thisinvestigation into the application of thermodynamic simulations to their behaviour under hightemperature,creep-like conditions. Precipitation sequences in the base metals, as well as carbonmigration in DMWs from the higher alloyed to the lower alloyed material at elevated temperatures, andthe distribution of precipitates across the fusion line of the DMWs, are all calculated using the softwareMatCalc. The simulation results are validated by testing creep-exposed cross-weld samples at 80 MPa,600 °C, and 625 °C for up to 14,000 hours.

Keywords: Ferritic steels , Dissimilar metal welds (DMWs), Carbon migration , Simulation

X

INTRODUCTION

Steels with increased creep strength, such as 9 wt% chromium Grade 91 and 2.25 wt% chromium Grade 23, have been made possible by the ever-increasing efficiency of today's fossil fuel power plants. These materials' extraordinary creep capabilities result from the interplay of several various types of strengthening processes, including dispersion hardening, solution hardening, and subgrain boundary hardening. When micro-alloying elements like vanadium, niobium, carbon, and nitrogen are added to a material, they generate carbides and carbonitrides that improve the bainitic microstructure [1]. However, the strength of Grade 91 materials comes from their precipitation-strengthened martensitic microstructure.

Dissimilar materials must be transitioned over short distances in today's power plants to satisfy a wide range of service conditions. To back up best practise fabrication, estimate remaining life, and back up future inspection decisions, knowing how dissimilar metal welds (DMW) behave under creep conditions is essential.

At high temperatures in service, a phenomena known as uphill-diffusion of carbon from the lower alloyed chromium steel to the one with greater chromium content can be observed [2–5]. This is caused by the rapid transition between materials with extremely different chemical compositions. Because of the differing chemical activities of carbon in the two materials employed in the DMW, carbon will migrate from one to the other, permanently altering the microstructure close to the fusion line. Carbon enrichment on the more highly alloyed side causes carbides to precipitate near the fusion line in the carbon enriched zone (CEZ), which depletes the surrounding matrix of carbide forming elements like chromium and consequently

changes the properties of this area relative to those of the base metal matrix. In contrast, carbon is depleted from the microstructure on the less alloyed side. In order to provide the carbon migration with atoms, a carbon-depleted zone (CDZ) is created where all the carbides are dissolved. However, at higher temperatures, the microstructure tends to recrystallize to a weaker ferritic crystal structure, as the carbides in the lower alloyed material no longer provide sufficient support for the martensitic/bainitic microstructure. These structural changes are localised to an area less than 1 mm across the fusion line, and they lead to a change in mechanical characteristics. As a result, strain localization can become more pronounced, making the component more vulnerable to damage under real-world conditions [6, 7].

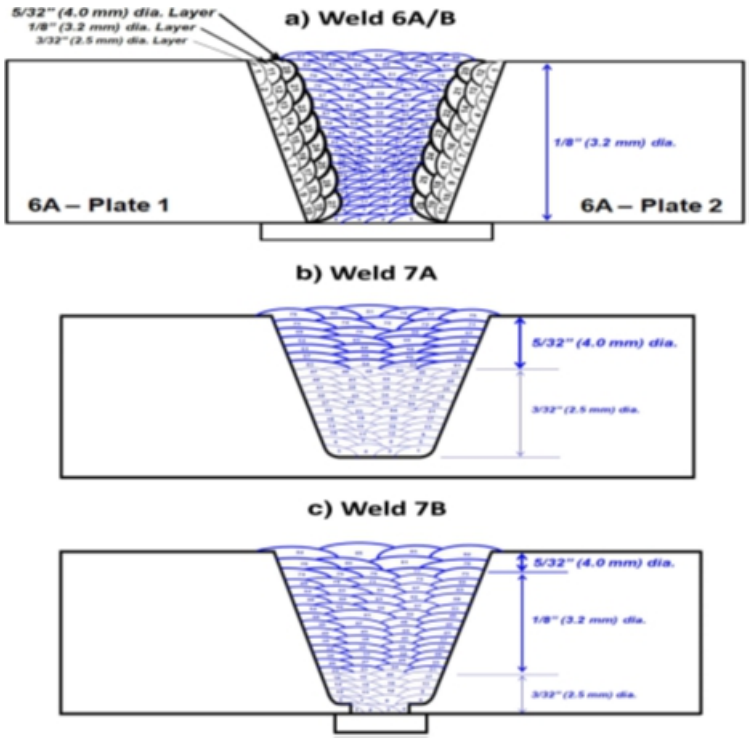

Figure 1: Schematics of the weld layer sequences for the feature sized creep samples

Table 1: Chemical compositions of the used materials in wt%; Fe balance; n.s. for "not specified"

Material	C	Cr	Mo	V	Mn	Ni	W	Si	N	Nb
Grade 23 dia. 4 mm	0.07	2.33	0.00	0.222	0.61	0.04	1.55	0.24	n.s.	n.s.
Grade 23 dia. 3.2 mm	0.07	2.28	0.01	0.19	0.52	0.08	1.73	0.23	n.s.	n.s.
Grade 23 dia. 2.5 mm	0.07	2.58	0.01	0.207	0.63	0.05	1.6	0.22	n.s.	n.s.
Grade 91 parent	0.11	8.29	0.95	0.2	0.45	0.14	---	0.29	0.0379	0.069
	Al	As	Cu	P	S	Sn	N:Al			
	0.006	0.005	0.16	0.011	0.009	0.01	6:3			

Table 2: Recorded weld parameters for the welds 6A/B, 7A, and 7B. The minimum to maximum range values rather than the specific values for amperage, voltage, weld speed, and heat input are given to keep a proper readability of the table

Weld	Dia. (mm)	Pass	Amperage (A)	Voltage (V)	Weld speed (cm/min)	Heat input (kJ/cm)
6A/B flanks	2.5	1&10/1&11	74–78	21–27	17.5–19	5.59–5.98
	3.2	11&19/12&19	111–113	22–24.1	18–19.6	7.52–8.66
	4.0	20&27/20&26	154–157	21–25	17.5–21.3	10.63–12.48
6A/B fill	3.2	1–94	125–126	24–25.2	17.3	10.71
7A fill	2.5	1–20	74–77	21–24	20	5.08
	3.2	21–72	111–113	22.3–25.4	19.6	8.22
	4.0	73–85	125–127	22–24.2	15.2	11.46
7B fill	3.2	1–50	97–98	23.1–24.5	16.3	8.62

EXPERIMENTAL PROCEDURES

Computing simulations were carried out using MatCalc Version 5.62 [8]. To learn about the precipitation habits of the materials, equilibrium phase fraction calculations were performed. Carbon activity calculations were also performed since carbon activ- ity variations in the material constitute the driving factor for carbon migration in DMWs [9]. In addition, a 1-dimensional finite ele- ment mesh with 100 elements was used to perform the diffusion calculations. Please note that the mc fe 2.058.tdb and mc fe 2.010.ddb MatCalc databases were used to perform the thermodynamic equilibrium and diffusion calculations, respectively, and that no user-specified parameters were used in either calculation. This paper's calculations are based on those of a different DMW [10].

Metallographic analysis of creep-tested cross-weld samples of T91 welded with T23 weld metal confirmed the accuracy of the calculations. For example, the most noticeable microstructure changes occur at the fusion line region between the T23 weld metal and the T91 base material when it is exposed to creep. There were Grade 23 weld metal electrodes and a Grade 91 base material, and their alloying compositions are summarised in Table 1.

Using three different Grade 23 type weld electrodes ("E9015-G") of varying electrode diameters, the welds were created by hand using manual shielded metal arc welding (SMAW) (2.5 mm, 3.2 mm, 4 mm). Sequence diagrams of the weld layers are depicted in Fig. 1. The thickness of the plate was 48 mm, the preheat temperature was 150 C, and the interpass temperature was 315 C. Table 2 provides a summary of the observed welding parameters; the "Pass"-column numbers correlate to the pass numbers shown in the layer sequence diagrams in Figure 1. Samples were PWHT at 745°C for 2 hours after welding. After being subjected to welding and PWHT, the samples were machined so that creep testing could take place. Sample geometries for creep testing at 600 and 625 degrees Celsius and 80 MPa are shown in Figure 2.

Next, EDM was used to cut the specimens after they had been subjected to creep. Samples were prepared for optical microscopy and hardness testing by normal metallographic procedure, which included grinding, polishing, and etching (Nital, 2%) the samples. For light-optical study, we employed a Zeiss Axiovert 200 MAT microscope, and for SEM examination, we utilised a Zeiss LEO 1400. A Struers DuraScan 7 was used to determine the material's hardness in accordance with DIN EN ISO 6507.

RESULTS AND DISCUSSION

Computational simulations

It is feasible to analyse equilibrium conditions to explain pre-cipitation behaviour during cooling of the base metals with only the chemical composition of the applied material. To do thermodynamic calculations, MatCalc employs the CALPHAD approach, which permits the user to add flexible databases for various alloying systems. Because of this, we can make predictions about material behaviour in settings when no experimental data exists. A large number of simulations can be computed if the chemical composition of the system is known. Precipitation patterns in the materials were estimated by simulating the equilibrium phase fractions. You can see the phase fraction diagram for Grade 23 weld metal in Figure 3.

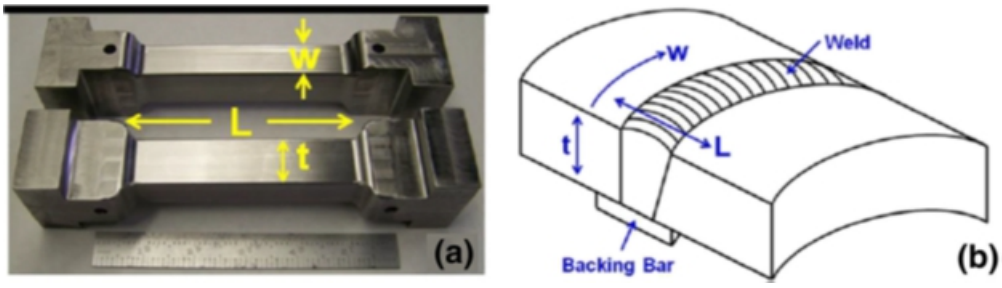

Figure 2: Machined feature-sized creep specimens (a) and relationship of orientation and geometry of the actual weld joint (b)

A wide range of precipitates was considered in the analyses. After reviewing the relevant literature [2, 5, 11–16], we learn that M23C6 carbides and MX carbonitrides are the most abundant precipitate species in the tested substances. Different studies have discovered both M6C and M7C3 carbides in low- and high-chromium-alloyed steels. Figure 3 shows a clear link between M7C3 and M23C6 precipitation. The simulation results indicate that M7C3 precipitation occurs during cooling after austenite transforms into ferrite. At temperatures of about 510 °C, M7C3 precipitates are being dissolved in favour of M23C6 carbides. The simulation findings demonstrate an earlier commencement of M23C6 precipitation at 780 °C if M7C3 carbides are not included in the calculations (Fig. 4). This illustration should make it clear that accurate material behaviour simulation requires knowledge of precipitates present in the materials.

The following carbon migration calculations are based on the carbon activity calculations performed on Grade 91 base metal and Grade 23 weld metal, respectively. Carbon activity findings for the sample materials are displayed in Figure 5. Compared to Grade 91 base material, Grade 23 weld metal electrodes have much lower carbon activity by more than an order of magnitude. What's fascinating is that despite the fact that the weld metal electrodes share a virtually identical chemical makeup, they have noticeably different carbon activity.

Considering the disparities in the weld metal electrodes' chemical makeup, it's intriguing to speculate on the feasibility of bridging the carbon activity gap by adjusting the electrodes' chemical makeups within the bounds of the materials' stipulated elements (see Table 3) [17, 18]. A reduction in the driving force for carbon migration will occur if the gap in carbon activity can be closed or at least substantially narrowed by altering the concentration of the alloying elements.

There needs to be an initial assessment of how various factors affect car- bon activity. One way to achieve

this is to change the content of just one element inside its defined borders while leaving the rest of the components unchanged. Carbon activity versus ele- ment content plots reveal how different elements affect carbon activity in a given substance (compare Fig. 6).

Calculations show that increasing the Cr, W, V, Mo, and Nb element contents while decreasing the C, N, and B element contents will reduce the carbon activity of Grade 23 material. The similar approach can be used to increase the carbon activity of Grade 91 material. What we get after the procedure is depicted in Fig. 7. The discrepancy between Grade 91 and Grade 23 materials' carbon activities cannot be eliminated entirely. At 550 °C, for instance, T23/T91 has a ratio of 51.25 (large gap) while T23v/T91v (materials with a tailored composition that is aimed to reduce the carbon activity difference) has a ratio of 3.33 (small gap). This reduction in the carbon activity ratio by a factor of 15 should significantly lessen the driving force for the carbon migration.

Table 3: Chemical composition boundaries (minimum and maximum allowable content) for Grade 23 and Grade 91 material in wt% according to [17, 18]

	C	Mn	Cr	Mo	Si	Ni	V	N	Nb/Ti
Grade 91	0.08–0.12	0.3–0.6	8.0–9.5	0.85–1.05	0.2–0.5	<0.4	0.18–0.25	0.03–0.07	0.06–0.1
	C	Mn	Cr	Mo	Si	Nb	V	N	W
Grade 23	0.04–0.1	0.1–0.6	1.9–2.6	0.05–0.3	<0.5	0.02–0.08	0.2–0.3	<0.03	1.45–1.75

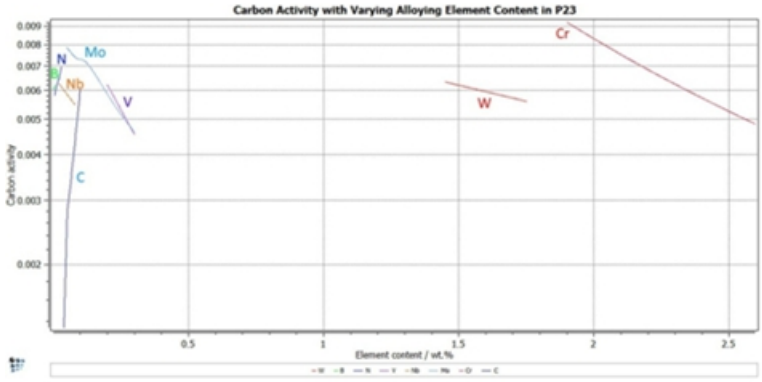

Figure 3: Influence of varying element content on the carbon activity of Grade 23 material

Metallographic investigation

To verify the results achieved via simulations, microstruc- tural investigations in the area of the fusion line with a light-optical microscope and SEM examination were carried out. Directed carbon migration from the lower alloyed weld metal to the higher alloyed base material caused negative microstructural changes as a result of the applied stress and the elevated temperature. As previously indicated, the carbon depletion leads to the breakdown of microstructure-stabilizing carbides in the Grade 23 weld metal which results in undesirable recrystallized ferrite in the carbon-depleted zone (CDZ) (CDZ). Furthermore, photos obtained using a scanning electron microscope support these results .This photo was captured by the SEM's secondary electron (SE) detector. On the T91 side, little finely scattered carbides may be recognised, while on the T23 side, very coarse structures are apparent. The creation of fine par- ticles in the Grade 91 material leads to a local increase in the hardness next to the fusion line, when on the contrary in the lower

alloyed weld metal, the carbon depletion weakens the microstructure and makes it softer. Based on EDS examination, the coarse white particles found on the Grade 23 weld metal side are Laves phase, which is rich in tungsten.

Weld metal microstructure has only undergone partial recrystallization, as shown by microstructural investigation, hence ferrite islands are only seen at the fusing point. Reasons for this include the use of micro-alloying to increase strength, and the minimal amount of time required for testing (1000 to 10,000 h). Table 4 is a summary of the information gathered about ferritic recrystallization. It is interesting to note that the diffusion and, ultimately, the recrystallization behaviour of the weld metal appear to be affected by the state of the Grade 91 base material. In contrast to the "B" samples, which were made using Grade 91 material that had been renormalized and tempered before welding, the "A" samples were made with untreated ex-service material.

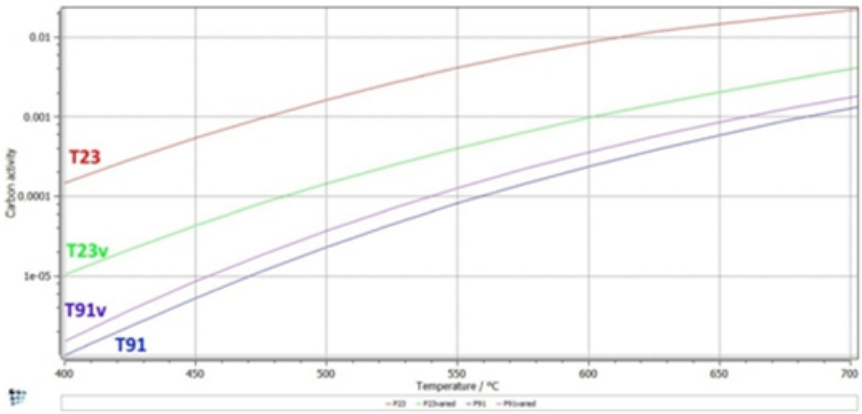

Figure 4: Carbon activity comparison for the investigated materials (T23 and T91) and materials with a tailored chemical composition that is aimed to reduce the carbon activity difference (T23v and T91v)

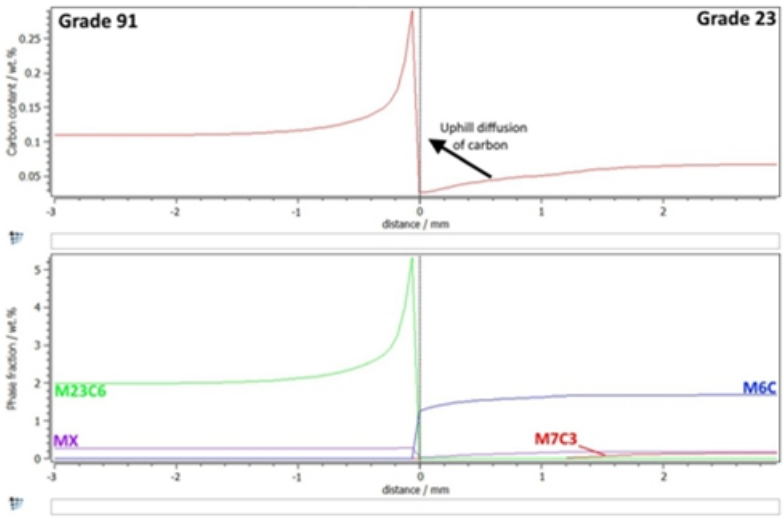

Figure 5: Diffusion calculation over the fusion line of a Grade 91 to Grade 23 DMW. Upper plot shows the carbon content after a simulated exposure of 2350 h at 625 °C. Bottom diagram shows the

corresponding response of phase fraction evolution of the different precipitates. The dotted line at 0 mm indicates the fusion line

After creep exposure, the renormalized and tempered samples clearly exhibit higher recrystallization than the untreated samples, despite the fact that the testing time for both groups was shorter. The normalising process is responsible for this improvement by decreasing the microstructure's dislocation density. It is possible to expedite the recrystallization process by increasing the temperature of the sample during the creep exposure so that more dislo- cations are formed and accumulated.

Evaluation of Toughness

The influence of PWHT and creep exposure on the welds was studied by measuring the joints' hardness. Renormalized and tempered Grade 91 base material appears to be slightly tougher than the ex- service ("A") sample, and this trend continues in the as-welded condition. There is not much of a distinction in the weld metal. Weld metal hardness decreases after PWHT, by 113 HV10 for "A" samples and 128 HV10 for "B" samples. There was a greater reaction to PWHT in the renormalized and temperature-treated base metal specimen, with a fall in hardness of 38 HV10, compared to the "A"- sample, which only showed a decrease in hardness of 22 HV10. Micro- hardness line scanning (HV0.05) across the fusion line of sample 7A-2 yielded the image in Fig. 11. There is a clear decrease in hardness on the weld metal side, and its breadth of around 100 m matches well with the width of the recrystallized microstructure. Finely distributed carbides precipitated across the fusing line as a result of carbon migration, creating a zone of increased hardness known as the carbon enriched zone (CEZ). The findings of the microstructural investigation and the outcomes of the computational simulations are corroborated by this line scan.

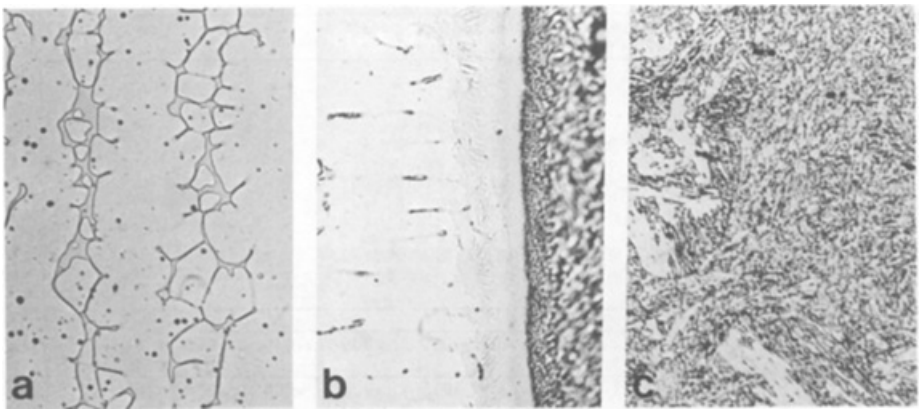

Figure 6: SEM picture of a creep exposed (600 °C for 7347 h) Grade 91 (T91) to Grade 23 (T23) DMW. SE image, red dotted line indicates the fusion line

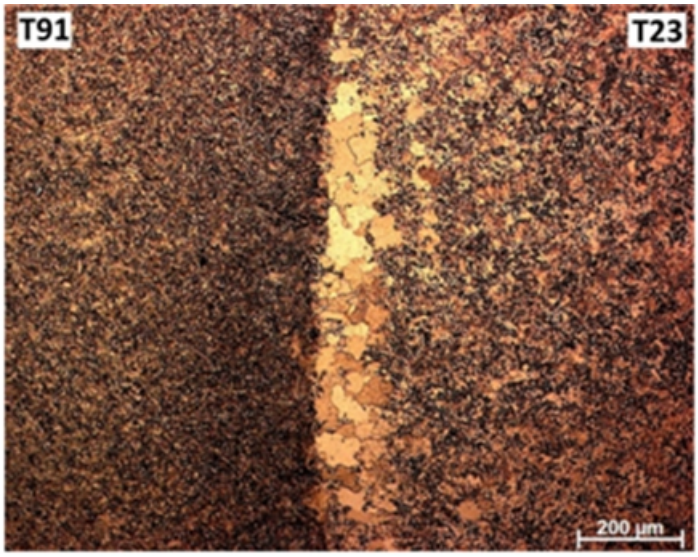

Figure 7: Partially recrystallized microstructure along the fusion line in the Grade 23 weld metal creep exposed for 2314 h at 625 °C

CONCLUSIONS

The purpose of this research was to illustrate the potential of using thermodynamic simulation software to predict the behaviour of creep-exposed dissimilar metal welds. Precipitation sequences during equilibrium cooling can be predicted by basing thermodynamic calculations on the chemical composition. These findings are useful inputs for more involved calculations like 1-dimensional diffusion simulations where the simulation parameters are set to mimic creep experiments or service conditions. Under conditions resembling those of real-world creep exposure tests, carbon migration calculations revealed the magnitude of carbon depletion in the lower alloyed material and carbon enrichment in the higher alloyed material. The extent of the difference between high- and low-chromium steels was calculated using carbon activity calculations. In addition, a concrete illustration of the usefulness of element activity calculations in the context of alloying optimization was provided.

The unfavourable microstructural changes that these welded joints undergo under service conditions were revealed by microstructural studies of creep-exposed T91 to T23 DMWs. The dissolution of carbides in the carbon-depleted zone resulted in a partial recrystallization of the weld metal microstructure. In addition, on the side of the weld that contains the more highly alloyed Grade 91 base metal, finely distributed carbides were discovered to correlate to a dramatic increase in hardness right next to the fusion line. Good agreement was found between the computational simulations and the creep experiments after an analysis and comparison with the data accumulated with 1-dimensional diffusion simulations. It was also demonstrated that familiarity with the materials and their precise microstructural features, specifically their inherent precipitate phases, is necessary for improved results from the computational simulations.

Table 4 Summary of collected hardness measurement data. WM Grade 23 weld metal, BM Grade 91 base metal

Sample		As welded			
		7A BM	7A WM	7B BM	7B WM
	Hardness / HV 10	206	323	260	352
Sample		After PWHT			
		7A BM	7A WM	7B BM	7B WM
	Hardness / HV 10	184	210	222	224
Sample ID	After creep exposure				
		7A-1 BM	7A-1 WM	7B-1 BM	7B-1 WM
	Hardness / HV 10	184	190	215	216
Sample ID		7A-2 BM	7A-2 WM	7B-2 BM	7B-2 WM
	Hardness / HV 10	182	192	207	195

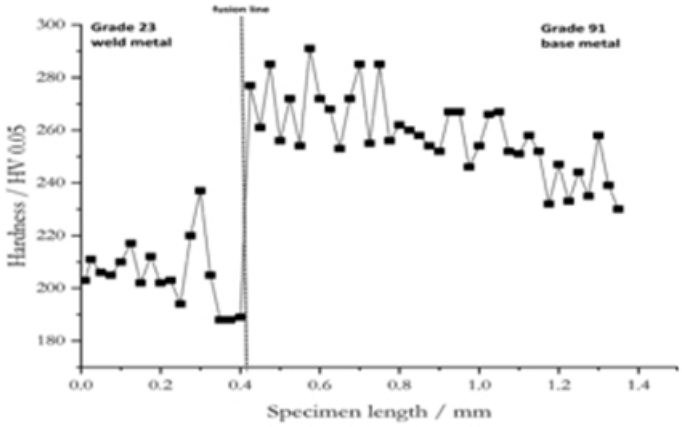

Figure 8: Microhardness line scan across the fusion line of the sample 7A- 2, through an area of recrystallized material

References

1. Vaillant JC, Vandenberghe B, Hahn B, Heuser H, Jochum C (2008) T/P23, 24, 911 and 92: new grades for advanced coal-fired power plants – properties and experience. Int J Press Vessel Pip 85:38–46. https://doi.org/10.1016/j.ijpvp.2007.06.011

2. Anand R, Sudha C, Saroja S, Vijayalakshmi M (2013) Experimental and thermokinetic simulation studies on the forma- tion of deleterious zones in dissimilar ferritic steel weldments. Metall Mater Trans A 44A:2156–2170. https://doi.org/10.1007/ s11661-012-1591-9

3. Dawson KE (2012) Dissimilar metal welds. Dissertation, University of Liverpool

4. Sudha C, Terrance ALE, Albert SK, Vijayalakshmi M (2002) Systematic study of formation of soft and hard zones in the dissim-ilar weldments of CrMo steels. J Nucl Mater 302:193–205. https:// doi.org/10.1016/S0022-3115(02)00777-8

5. Sudha C, Thomas Paul V, Terrance ALE, Saroja S, VijayalakshmiM (2006) Microstructure and microchemistry of hard zone in dis- similar weldments of Cr-Mo steels. Weld J:71–80

6. Thomas A, Pathiraj B, Veron P (2007) Feature tests on welded components at higher temperatures – material performance and residual stress evaluation. Eng Fract Mech 74:969–979. https://

doi.org/10.1016/j.engfracmech.2006.08.017

7. Wang Y, Li L (2016) Microstructure evolution of fine-grained heat affected zone in type IV failure of P91 welds. Weld J 95:27–36
8. E. Kozeschnik: MatCalc (Materials Calculator); software available athttps://www.matcalc-engineering.com/index.php. Accessed 20 Oct 2019
9. Darken LS (1949) Diffusion of carbon in austenite with a discontinuity in composition. Trans AIME 180:430–438
10. Dittrich F, Mayr P, Martin D, Siefert JA (2018) Characterization of an ex-service P22 to F91 ferritic dissimilar metal weld. Weld World 62:793–800. https://doi.org/10.1007/s40194-018-0569-7.
11. Strilkova L, Kubon Z, Vodarek V (2010) Creep failure characteris- tics in P23/P91 dissimilar welds. Conference Paper - METAL 2010.
12. Amsupan S, Consonni M, Poopat B, Sirivedin K (2015) Influence of the welding heat cycle on the HAZ properties of T23 joints. Int J Inst Mater Malays 2-1:233–24
13. Dawson K, Tatlock G (2011) The stability of fine, sub-grain micro- structures within carbon depleted regions of dissimilar metal, ferrit- ic, creep resistant welds. ASME 2011 pressure vessels and piping conference. https://doi.org/10.1115/PVP2011-57868
14. Laha K (2014) Integrity assessment of similar and dissimilar fusion welded joints of Cr-Mo-W ferritic steels under creep condition. Proc Eng 86:195–202. https://doi.org/10.1016/j.proeng.2014.11. 028.
15. Foret R, Zlamal B, Sopousek J (2006) Structural stability of dissimilar weld between two CrMoV steels. Weld J:211–217.
16. Vodarek V, Kubon Z, Foret R, Hainsworth SV (2008) Microstructural evolution in P23/P91 heterogeneous welds during creep at 500-600°C. Safety and reliability of welded components in energy and processing industry proceedings of the IIW international conference, pp 233–238.
17. Case 2199: 9Cr-1Mo-1W-Cb Material, Cases of American Society of Mechanical Engineers Pressure Vessel, Code Case 2199–6, 2011 DIN EN 10302:2008–06 – Creep resisting steels, nickel and cobalt alloys